nature communications

Article

https://doi.org/10.1038/s41467-022-32677-3

Ultramicroporous material based parallel and extended paraffin nano-trap for benchmark olefin purification

Received: 16 March 2022

Accepted: 11 August 2022

Published online: 22 August 2022

Check for updates

Peixin Zhang[1,2], Lifeng Yang[1], Xing Liu[3], Jun Wang[3], Xian Suo[2], Liyuan Chen[1], Xili Cui[1,2] & Huabin Xing[1,2]

Selective paraffin capture from olefin/paraffin mixtures could afford high-purity olefins directly, but suffers from the issues of low separation selectivity and olefin productivity. Herein, we report an ultramicroporous material (PCP-IPA) with parallel-aligned linearly extending isophthalic acid units along the one-dimensional channel, realizing the efficient production of ultra-high purity C_2H_4 and C_3H_6 (99.99%). The periodically expanded and parallel-aligned aromatic-based units served as a paraffin nano-trap to contact with the exposed hydrogen atoms of both C_2H_6 and C_3H_8, as demonstrated by the simulation studies. PCP-IPA exhibits record separation selectivity of 2.48 and separation potential of 1.20 mol/L for C_3H_8/C_3H_6 (50/50) mixture, meanwhile the excellent C_2H_6/C_2H_4 mixture separation performance. Ultra-high purity C_3H_6 (99.99%) and C_2H_4 (99.99%) can be directly obtained through fixed-bed column from C_3H_8/C_3H_6 and C_2H_6/C_2H_4 mixtures, respectively. The record C_3H_6 productivity is up to 15.23 L/kg from the equimolar of C_3H_8/C_3H_6, which is 3.85 times of the previous benchmark material, demonstrating its great potential for those important industrial separations.

Olefins (e.g., propylene and ethylene) are important chemical feedstocks in petrochemical industry, and at least polymer-grade or even the ultra-high purity (99.99%) olefins are required for the manufacture of advanced fine chemicals and polymers[1,2]. Olefin/paraffin separation is the key process to afford high purity olefins, but is mainly carried out via cryogenic distillation that is associated with high energy footprints, or even the multistep distillation[3–5]. The development of non-thermal driven alternatives with low carbon emissions are the potential solutions to the challenges[5,6].

Adsorptive separation technologies based on porous materials provide a feasible avenue to solve the dilemma, and the technologies show more attractive prospects with the continuous progress in tailor-made porous materials[7–14]. Olefin-selective adsorbents have been widely explored for olefin/paraffin separation with considerable achievements[15–24]. However, even the current benchmark molecular-sieving material with ideally infinite olefin/paraffin selectivity could only afford olefins with purity of 99.1% due to the inevitable coadoption of paraffins, and extra adsorption–desorption cycles are necessary for olefins to reach polymer-grade purity[17]. It is rationally speculated that the purification steps would be more complex to produce olefins with ultra-high purity (99.99%)[25,26]. By contrast, paraffin-selective adsorbents are advantaged in directly affording high-purity olefins via only single adsorption cycle, simplifying the separation process, and gradually attract the interests[27–30]. For example, Hartmann et al. reported two Zeolite imidazolate frameworks (ZIF-4 and ZIF-8) showed stronger affinity toward alkanes than alkenes[31,32], Jorge et al. proved that ZIF-7 could selectivity adsorbed alkanes over alkenes through gate-opening effect[33], and Anne et al. predicted Silicalite-1 possess paraffin-selective adsorption performance[34]. As evidence of the reported paraffin-selective adsorbents, there are two

[1]Key Laboratory of Biomass Chemical Engineering of Ministry of Education, College of Chemical and Biological Engineering, Zhejiang University, Hangzhou 310027, Zhejiang, P. R. China. [2]ZJU-Hangzhou Global Scientific and Technological Innovation Center, Hangzhou 311215, Zhejiang, P. R. China. [3]Chemistry and Chemical Engineering School, Nanchang University, Nanchang 330031, Jiangxi, P. R. China. e-mail: xinghb@zju.edu.cn

ways to realize the selective adsorption of alkanes. (1) Through the construction of specific functional sites and the control of functional sites distribution to form multiple hydrogen-bond with paraffins, such as the iron-peroxo sites of $Fe(O_2)(dobdc)$[35], the precise N and O distribution of MAF-49[36] and JNU-2[37], etc.[38,39], exhibit higher affinity to C_2H_6 than C_2H_4. (2) Enriching with the nonpolar surfaces of pore structure to recognize the paraffins and olefins properties difference of quadrupole moment, like BUT-10[40], PCN-250[41], $Cu(Qc)_2$[42], HOF-76[43], and etc.[44–47]. However, most of these paraffin-selective adsorbents design approaches are based on the three dimensions of pore to match the size of paraffins, it reversely causes the inefficiency of single material to simultaneously identify C_2H_6 and C_3H_8 with different molecular size (Fig. 1a). In addition, though the remarkable progress in the design, both separation selectivity and olefin productivity of the current paraffin-selective adsorbents are still to be improved, especially for C_3H_8/C_3H_6 mixture, the paraffin/olefin selectivity is below 2, and the olefin productivity is lower than 4.0 L/kg[40,48–50].

Considering the preferential paraffin adsorption behavior is dominated by the interactions between the hydrogen atoms of paraffins and the framework, and the similar structural conformation of C_2H_6 and C_3H_8 in the specific orientation with both side-distributed hydrogen atoms that are easily accessible, a parallel and extended paraffin nano-trap would be favored for paraffin accommodation via the close and dense contact with the hydrogen atoms (Fig. 1b). Herein, we reveal that the ultramicroporous material $[Co(IPA)(DPG)]_n$ (PCP-IPA; PCP = Porous coordination polymer, IPA = isophthalic acid, DPG = meso-α, β-di(4-pyridyl) glycol) featuring with parallel-aligned linearly extending isophthalic acid units sets a new benchmark for paraffin/olefin separations. The unique pore size and environment enables the directional adsorption of C_2H_6 and C_3H_8 through the rigidly bounded between their aligned hydrogen atoms and the closely parallel-aligned isophthalic acid units, realizing the simultaneous efficient separation of both C2 and C3 paraffin/olefin mixtures. PCP-IPA exhibits the record C_3H_8/C_3H_6 selectivity of 2.48 and separation potential of 1.20 mol/L for C_3H_8/C_3H_6 (50/50) mixtures, as well as the excellent C_2H_6/C_2H_4 separation performance. Ultra-high purity C_3H_6 (99.99%) and C_2H_4 (99.99%) are obtained through the breakthrough experiment using PCP-IPA from C_3H_8/C_3H_6 and C_2H_6/C_2H_4 mixture, respectively. The record C_3H_6 productivity is up to 15.23 L/kg from the equimolar of C_3H_8/C_3H_6, 3.85 times of the previous benchmark material. The molecular-level insight into the paraffin and olefin adsorption behaviors are further revealed by simulation studies.

Results

Synthesis and characterization

The reaction of meso-α, β-di(4-pyridyl) glycol (DPG), and isophthalic acid (IPA) with $Co(NO_3)_2{\cdot}6H_2O$ afforded PCP-IPA[51]. Individually, in PCP-IPA, each Co(II) atom is six coordinated in an octahedral geometry, and the coordination between the Co atoms and two N atoms from the pyridine ring, two O atoms from the hydroxyl group of the DPG ligand forms a 2D layer network (Supplementary Fig. 2). The adjacent 2D layer networks are pillared with the IPA ligands to afford a 3D pillared layered framework with one-dimensional straight channel (Fig. 1c, d). The channel is featured with the parallel-aligned linearly extending isophthalic acid units, and the pore window of PCP-IPA is estimated to be 4.7×5.6 Å^2, which is suitable for the accommodation of paraffins. Benefiting from the big π system and hydrogen bond acceptor provided by the aromatic units and uncoordinated negatively charged oxygen atoms, the channel is anticipated to be an efficient paraffin nano-trap. The experimental PXRD pattern of PCP-IPA matches well with the simulated one, confirming the high phase-purity of as-synthesized PCP-IPA (Supplementary Fig. 3). PCP-IPA shows good thermal stability up to 280 °C (Supplementary Fig. 4). The permanent pore structure of PCP-IPA is investigated by 195 K CO_2 adsorption–desorption isotherm (Supplementary Fig. 5), and the Langmuir-specific surface area and pore volume of PCP-IPA are determined as 486.7 m^2/g and 0.19 cm^3/g, respectively. Furthermore, the other basic characterization of SEM and FT-IR on PCP-IPA shown as Supplementary Figs. 6 and 7.

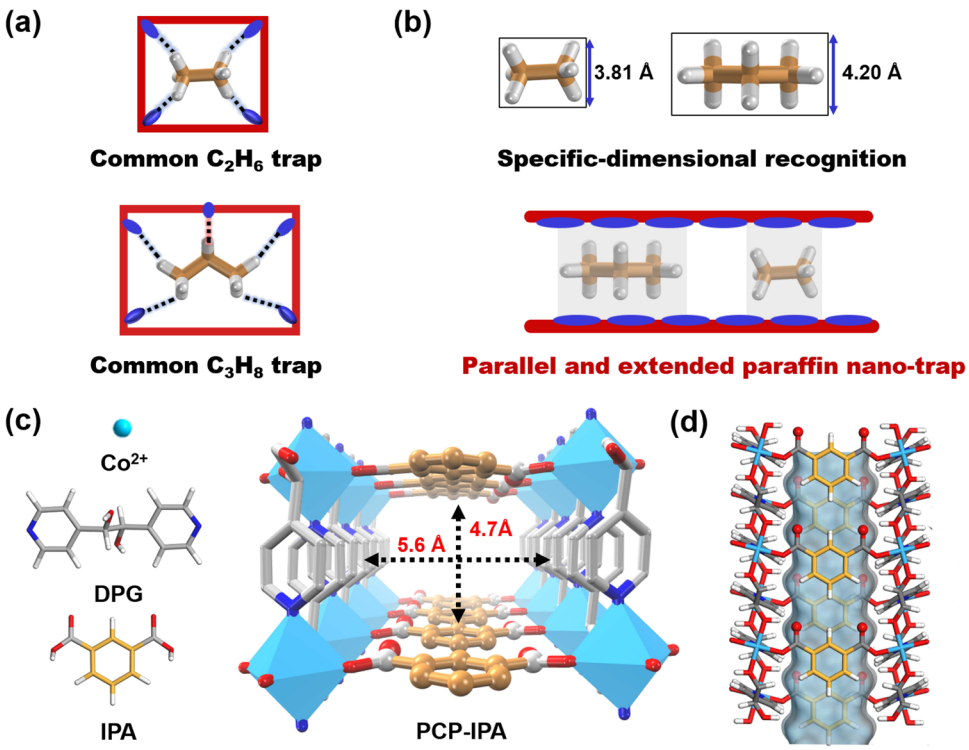

Fig. 1 | Scheme and structure of PCP-IPA. a Schematic illustration of the common paraffin-trap channel, **b** schematic illustration of the parallel and extended paraffin nano-trap channel, (**c**) the building blocks (Co^{II}, DPG, and IPA organic ligand) and the 3D network topology of PCP-IPA, **d** the 1D channel structure of PCP-IPA (C, orange or grey-80%; H, white; N, blue; O, red; Co, light blue).

https://doi.org/10.1038/s41467-022-32677-3

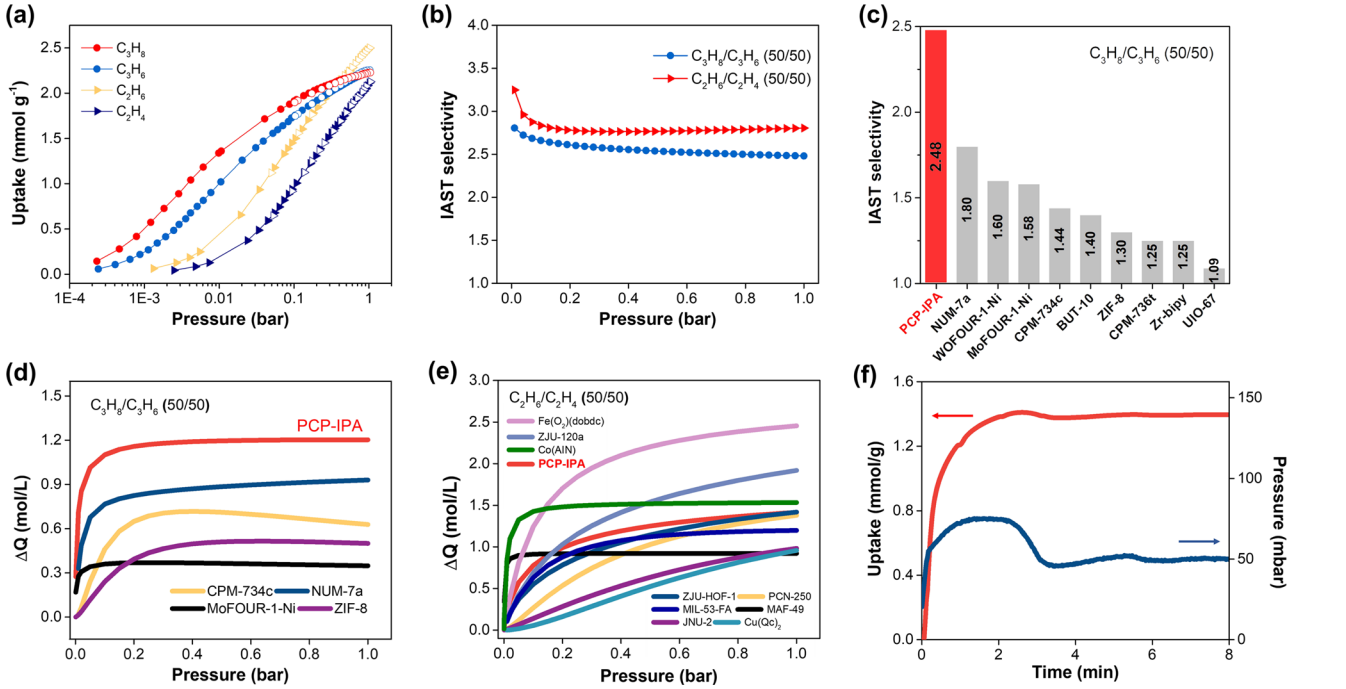

Fig. 2 | The paraffin and olefin sorption in PCP-IPA. a The C_3H_8, C_3H_6, C_2H_6, and C_2H_4 adsorption isotherms at 298 K; **b** IAST selectivity (**c**) comparison plot of C_3H_8/C_3H_6 (50/50 v/v) IAST selectivity among benchmark materials; comparison of PCP-IPA separation potential (ΔQ_{IAST}) with reported benchmark MOFs based on IAST calculation from **d** C_3H_8/C_3H_6 (50/50 v/v) mixtures and **e** C_2H_6/C_2H_4 (50/50 v/v) mixtures. **f** Time-dependent gas uptake profiles of C_3H_8 at 50 mbar and 298 K.

Adsorption and separation performances

The single-component adsorption isotherms were conducted to explore the paraffin/olefin separation performance of PCP-IPA (Fig. 2a and Supplementary Fig. 8). As expected, PCP-IPA exhibits remarkable paraffin-selective adsorption during the whole pressure range (0–1.0 bar). It sets a new benchmark IAST (Ideal adsorbed solution theory) selectivity for C_3H_8/C_3H_6 (50/50) up to 2.48 at 1.0 bar and 298 K (Fig. 2b), greater than the previously reported top-performing porous materials, such as NUM-7a (1.80)[50], WOFOUR-1-Ni (1.60)[48], CPM-734c (1.44)[49], and BTU-10 (1.40)[40] (Fig. 2c). Furthermore, the C_3H_8/C_3H_6 (50/50) separation potential ($\triangle Q$) that based on the combined effect of adsorption capacity and selectivity for separation performance prediction is revealed, and PCP-IPA also exhibits the record value, up to 1.20 mol/L (1.0 bar), 1.3 times to the previous benchmarks NUM-7a (0.93 mol/L) (Fig. 2d). Meanwhile, high separation selectivity up to 2.80 and separation potential ($\triangle Q$) for C_2H_6/C_2H_4 (50/50) mixture are also observed on PCP-IPA (Fig. 2e), highlighting the great separation potential of PCP-IPA for both C_3H_8/C_3H_6 and C_2H_6/C_2H_4 mixtures[52–55]. The higher affinity of paraffins to olefins is also verified by the calculated adsorption heat Q_{st} (C_3H_8 50.94 kJ/mol vs 43.36 kJ/mol, C_2H_6 37.73 kJ/mol vs C_2H_4 27.48 kJ/mol) (Supplementary Figs. 9 and 10). The kinetic effect is regarded as a great hindrance to prevent preferential paraffin adsorption behavior, and gas diffusion is a critical factor in ultramicroporous adsorbent for real industrial applications, the time-dependent gas uptake profiles of C_3H_8, C_3H_6, C_2H_6, and C_2H_4 were measured. The results show that the diffusion rates of all gases in the channel are fast and there are no kinetic difference between paraffins and olefins (Fig. 2f and Supplementary Fig. 12), demonstrating the suitable pore size of PCP-IPA.

Modeling simulation studies

To understand the molecular-level paraffin and olefin adsorption behavior within the channel of PCP-IPA, we performed detailed modeling studies using first-principles dispersion-corrected density functional theory (DFT-D) method. As shown in Fig. 3, the paraffins prefer the adsorbed orientation that the section of the molecules is vertical to the extending direction of the channel, and the parallel-aligned isophthalic acid units are served as the tailored binding environment for the lined hydrogen atoms of paraffins. Despite the different molecular lengths, C_2H_6 and C_3H_8 could collect enough binding sites along the extending isophthalic acid units, allowing PCP-IPA to have both high C_3H_8 and C_2H_6 affinity. Meanwhile, the pore structure of parallel-aligned linearly extending aromatic units as well as the appropriate distance between parallel benzene rings also give full play of the advantages of paraffins to olefins, the more C-H binding sites and large molecular size. Paraffins exhibit more dense interactions with the isophthalic acid units than olefins, which are also supported by the calculated binding energies of C_3H_8 (−54.01 kJ/mol), C_3H_6 (−50.32 kJ/mol), C_2H_6 (−39.36 kJ/mol), and C_2H_4 (−35.24 kJ/mol). In detail, each C_3H_8 molecule interacts with three phenyl rings and three uncoordinated oxygen atoms to form multiple van der Waals forces (eleven C-H•••C 2.83–3.21 Å) and three C-H•••O H-bonding interactions (C-H•••O 2.76–3.20 Å) (Fig. 3a). In contrast, the C_3H_6 molecule shows only one C-H•••O H-bonding interaction (C-H•••O 2.51 Å), and seven C-H•••C van der Waals forces (C-H•••C 2.80–3.16 Å) with framework (Fig. 3b). C_2H_6 shows the similar adsorption behavior, and is rigidly bounded by the more C-H•••C and C-H•••O interactions than C_2H_4 (Fig. 3c, d). The simulation studies reveal that the parallel-lined and linear-extending aromatic units could provide enough binding sites toward paraffins even with different molecular size thanks to the specific adsorbed orientation.

Transient breakthrough experiments

Furthermore, the dynamic transient breakthrough experiments were conducted to evaluate the actual separation ability of PCP-IPA for paraffin/olefin mixtures, and highly efficient separation performance is observed for both C2 and C3 paraffin/olefin separations. As the C_3H_8/C_3H_6 (50/50, v/v) mixture flows through the column packed with PCP-IPA, C_3H_6 is first eluted at the time of 34.8 min while C_3H_8 is continuously adsorbed until the time of 43.9 min (Fig. 4a). During the above time gap (34.8–43.9 min), ultra-high purity C_3H_6 (99.99%) can be collected with the record C_3H_6 productivity of 15.23 L/kg. The

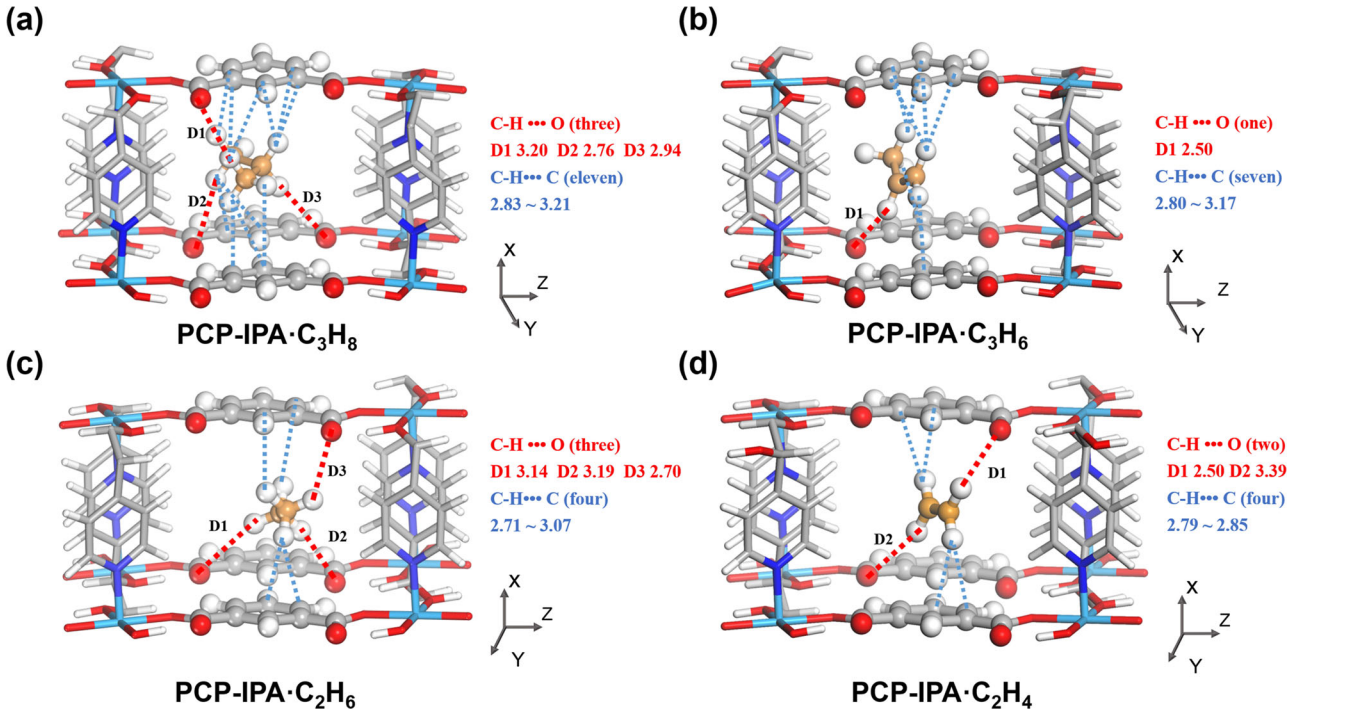

Fig. 3 | DFT-D calculated preferable binding sites for paraffins and olefins in PCP-IPA. a C_3H_8, **b** C_3H_6, **c** C_2H_6, and **d** C_2H_4 binding sites in PCP-IPA. The closest contacts between framework atoms and the gas molecules are defined by the distances (in Å) and the distances include the Van der Waals radius of atoms. (Framework: C, gray-80%; H, white; N, blue; O, red; Co, light blue; Gas: C, orange; H, white).

productivity is nearly four times that of the pervious benchmark material BUT-10 (3.95 L/kg)[40] and WOFOUR-1-Ni (3.50 L/kg)[48] under the same conditions. For C_3H_8/C_3H_6 mixtures with only 5% C_3H_8, we are still able to collect the 99.99% C_3H_6 and high C_3H_6 productivity of 30.06 L/kg, demonstrating the broad applicability of PCP-IPA for paraffin/olefin mixtures of different compositions. Consistent with the adsorption isotherms and simulation studies, PCP-IPA also shows remarkable C_2H_6/C_2H_4 separation performance and the corresponding C_2H_4 productivity is 26.2 L/kg, rendering it to be one of the leading materials for C_2H_6-selective adsorbents. In addition, we find that the paraffin working capacity of PCP-IPA calculated by breakthrough curves is close to the static adsorption capacity (C_2H_6, 2.10 vs 2.24 mmol/g; C_3H_8, 1.81 vs 2.16 mmol/g), further verifying the rapid diffusion behavior of paraffins and olefins within the channel (Supplementary Tables 6 and 7). We evaluate the influence of water vapor on the separation ability of PCP-IPA, and no decrease is observed on the breakthrough performance (Fig. 4c and Supplementary Fig. 18a). During the 14 cycling tests, the separation performance is well maintained (Fig. 4f, Supplementary Figs. 19–21 and Table 8). Meanwhile, PCP-IPA is also highly resistant to air and water, and both the XRD patterns and C_2H_6 capacity remain unchanged after treatment (Supplementary Fig. 17). The adsorption column could be regenerated rapidly and completely within 60 min and 45 min for C2 and C3 mixtures, respectively, under 333 K and 373 K with the purging N_2 flow rate of 10 mL/min (Supplementary Figs. 22 and 23). The impressive separation performance and the good stability of PCP-IPA highlight its great promise in paraffin/olefin separations.

Discussion

In summary, we have discovered a distinctive ultramicroporous material featuring closely packed and linearly-extended isophthalic acid units that realized the both efficient C2 and C3 paraffin preferential adsorption, respectively. The findings reveal an effective strategy to improve the affinity between paraffins and the frameworks through the construction of the periodically expanded and parallel-aligned aromatic-based units along the channel. Our developed material could produce ultra-high purity (99.99%) olefins, and the excellent paraffin/olefin separation selectivity and olefin productivity also well demonstrate the superiority of the strategy. This work not only presents a new benchmark porous material for paraffin/olefin separation, but will facilitate the future design of novel paraffin-selective materials for energy-efficient separations.

Methods

Chemicals

All reagents were analytical grade and used as received without further purification. $Co(NO_3)_2{\cdot}6H_2O$, Isophthalic acid (IPA), methanol (MeOH), and dimethylformamide (DMF) were purchased from Aladdin Reagent Co. Ltd., Meso-α,β-Di(4-pyridyl) Glycol (DPG) was purchased from TCI Co. Ltd. Ultra-high purity grade He (99.999%), N_2 (99.999%), C_2H_4 (99.99%), C_2H_6 (99.99%), C_3H_6 (99.99%), C_3H_8 (99.99%), CO_2 (99.999%), and mixed gases (C_2H_4/C_2H_6 = 50/50, *v/v*, C_2H_4/C_2H_6 = 15/1, *v/v*, C_3H_6/C_3H_8 = 50/50 *v/v*, C_3H_6/C_3H_8 = 95/5 *v/v*) were purchased from Shanghai Wetry Standard gas Co., Ltd. (China) and used for all measurements.

Preparation of the powder of PCP-IPA

PCP-IPA was synthesized according to the previously reported procedure[51]. 81 mg DPG was dissolved in DMF/MeOH (1:1, 30 mL) at 60 °C, and 62 mg IPA and 109 mg $Co(NO_3)_2{\cdot}6H_2O$ was dissolved in 5 mL MeOH. Then the two solutions were mixed and heated at 80 °C for 24 h hours to yield as-synthesized of PCP-IPA.

Sample characterization

Powder X-ray diffraction (XRD) patterns were collected using a PANalytical empyrean series2 diffractometer with Cu-Ka radiation, at room temperature, with a step size of 0.0167°, a scan time of 15 s per step, and 2θ ranging from 5 to 50°. The morphology was investigated using a NOVA 200 Nanolab scanning electron microscope (SEM). Fourier transform infrared (FTIR) spectra was recorded in the range of

https://doi.org/10.1038/s41467-022-32677-3

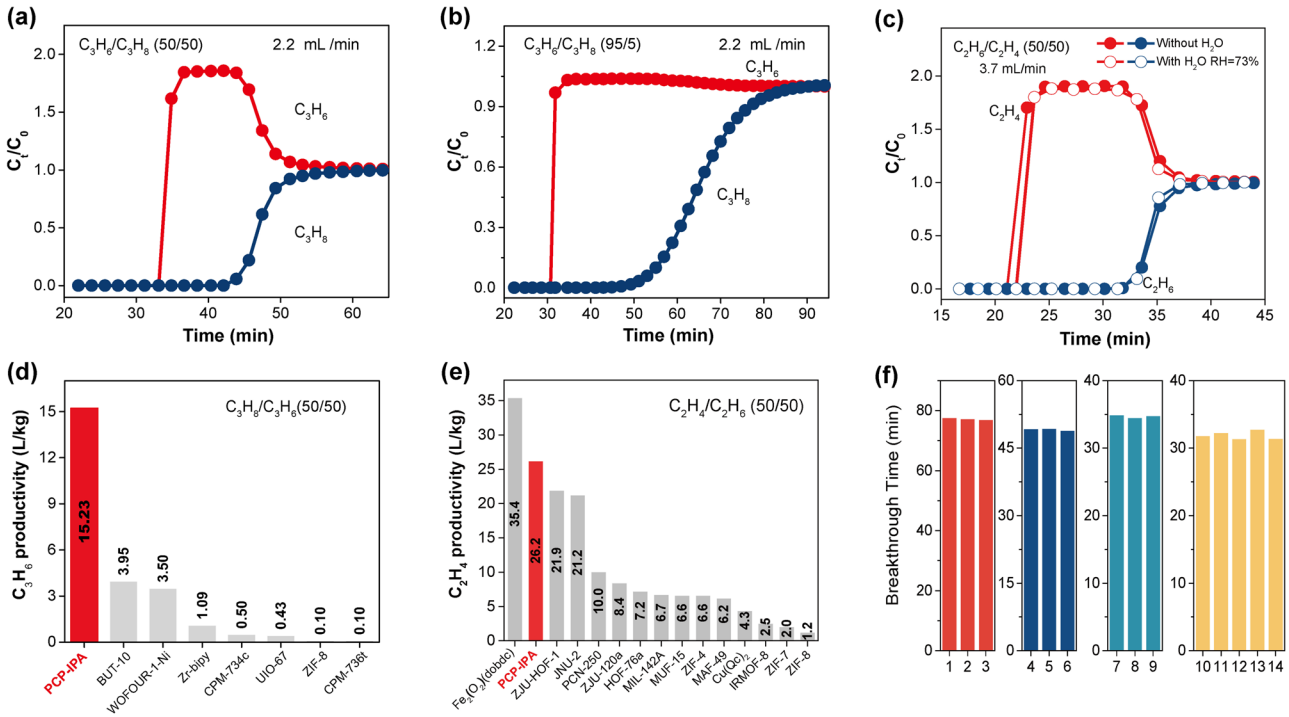

Fig. 4 | Paraffin/olefin separation. Dynamic breakthrough curves under 298 K and 1.0 bar of **a** C_3H_8/C_3H_6 (50/50 *v/v*) mixture, **b** C_3H_8/C_3H_6 (5/95 *v/v*) mixture, and **c** C_2H_6/C_2H_4 (50/50 *v/v*) with (hollow) or without water vapor (solid); comparison of high pure olefin productivity on PCP-IPA with reported benchmark materials for **d** C_3H_8/C_3H_6 (50/50 *v/v*) mixture and **e** C_2H_6/C_2H_4 (50/50 *v/v*) mixture; **f** recycling breakthrough tests for C_3H_8/C_3H_6 (5/95 *v/v*, red, 2.20 mL/min), C_3H_8/C_3H_6 (50/50 *v/v*, blue, 1.10 mL/min), C_3H_8/C_3H_6 (50/50 *v/v*, cyan, 2.20 mL/min) and C_2H_6/C_2H_4 (50/50 *v/v*, orange, 3.7 mL/min) separation with PCP-IPA under 298 K and 1.0 bar.

400–4000 cm^{-1} on a Nicolet 5700 FTIR spectrometer using KBr pellets. The thermogravimetric analysis (TGA) data were collected in a NETZSCH Thermogravimetric Analyzer (STA2500) from 25 to 700 °C with a heating rate of 10 °C/min. The CO_2 adsorption/desorption isotherms at 195 K were obtained on a Micromeritics ASAP 2460 volumetric adsorption apparatus. The apparent Langmuir-specific surface area was calculated using the adsorption branch with the relative pressure P/P_0 in the range of 0.005 to 0.1. The total pore volume (V_{tot}) was calculated based on the adsorbed amount of CO_2 at the P/P_0 of 0.99. The pore size distribution (PSD) was calculated using the H-K methodology with CO_2 adsorption isotherm data and assuming a slit pore model.

Gas adsorption measurements

The C_2H_4, C_2H_6, C_3H_6, and C_3H_8 adsorption–desorption isotherms at different temperatures were measured volumetrically by the Micromeritics ASAP 2460 adsorption apparatus for pressures up to 1.0 bar. The time-dependent gas uptake profiles of C_2H_4, C_2H_6, C_3H_6, and C_3H_8 were measured by Intelligent gravimetric adsorption (IGA-100, Hiden). Prior to the adsorption measurements, the samples were degassed using a high vacuum pump (<5 μm Hg) at 373 K for over 12 h.

Breakthrough experimental

The breakthrough experiments were carried out in a home-made apparatus. The sample was dried under vacuum at 100 °C for 12 h. Samples (about 1.29 g) were then introduced to the adsorption bed (φ6 mm × 150 mm). A carrier gas (He ≥99.999%) was used to purge the adsorption bed for more than 1 h to ensure that the adsorption bed was saturated with He. Then the gas flow is switched to the desired gas mixture without any inert gas dilution (C_2H_4/C_2H_6 = 50/50, *v/v*, C_2H_4/C_2H_6 = 15/1, *v/v*, C_3H_6/C_3H_8 = 50/50 *v/v*, C_3H_6/C_3H_8 = 95/5 *v/v*) at a certain flow rate. The recovery gas was passed to an analyzer port and analyzed using gas chromatography (GC490 Agilent) with a thermal conductivity detector (TCD). After breakthrough experiment, the adsorption column was regenerated at 100 °C with the 10 mL/min N_2 flow rate for 2 h.

Isotherm fitting

The pure-component isotherms of C_2H_6, C_2H_4, C_3H_8, and C_3H_6 were fitted using single-site Langmuir-Freundlich model for full range of pressure (0–1.0 bar).

$$q = q_{sat1}\frac{b_1 p^{v1}}{1 + b_1 p^{v1}} \tag{1}$$

here, p is the pressure of the bulk gas at equilibrium with the adsorbed phase (bar), q is the adsorbed amount per mass of adsorbent (mmol g^{-1}), q_{sat} is the saturation capacities (mmol g^{-1}), b is the affinity coefficient (bar^{-1}), and v represent the deviation from an ideal homogeneous surface.

Isosteric heat of adsorption

The isosteric heat of C_2H_4, C_2H_6, C_3H_6, and C_3H_8 adsorption, Q_{st}, defined as

$$Q_{st} = RT^2\left(\frac{\partial \ln P}{\partial T}\right)_q \tag{2}$$

were determined using the pure component isotherm fits using the Clausius-Clapeyron equation. where Q_{st} (kJ/mol) is the isosteric heat of adsorption, T (K) is the temperature, P (bar) is the pressure, R is the gas constant, and q (mmol/g) is the adsorbed amount.

IAST calculations

The selectivity of the preferential adsorption of component 1 over component 2 in a mixture containing 1 and 2 can be formally defined

as:

$$S = \frac{x_1/y_1}{x_2/y_2} \quad (3)$$

In the above equation, x_1 and y_1 (x_2 and y_2) are the molar fractions of component 1 (component 2) in the adsorbed and bulk phases, respectively. We calculated the values of x_1 and x_2 using the ideal adsorbed solution theory (IAST) of Myers and Prausnitz[56].

Separation potential calculation based on IAST

This separation potential, $\triangle Q$, represents the maximum number of moles of pure component 2 (the less strongly adsorbed species) that can be recovered in the gas phase per gram of adsorbent in the fixed bed. The separation potential of adsorbers in fixed bed for paraffin/olefin separation is defined by[57]

$$\triangle Q = q_1 - q_2 \frac{y_1}{y_2} \quad (4)$$

where q_1 and q_2 are the molar loadings for mixture adsorption, calculated from the IAST in mmol/g, y_2 and y_1 are molar fractions in the binary mixture gas.

Density functional theory calculations

First-principles density functional theory (DFT) calculations were performed using the Materials Studio's CASTEP code[58]. All calculations were conducted under the generalized gradient approximation (GGA) with Perdew–Burke–Ernzerhof (PBE). A semiempirical addition of dispersive forces to conventional DFT was included in the calculation to account for van der Waals interactions. Cutoff energy of 544 eV and a $2 \times 2 \times 2$ k-point mesh was found to be enough for the total energy to coverage within 0.01 meV atom^{-1}. The structures of the synthesized materials were first optimized from the reported crystal structures. To obtain the binding energy, the pristine structure and an isolated gas molecule placed in a supercell (with the same cell dimensions as the pristine crystal structure) were optimized and relaxed as references. C_2H_4, C_2H_4, C_3H_6, and C_3H_8 gas molecules were then introduced to different locations of the channel pore, followed by a full structural relaxation. The static binding energy was calculated by the equation:

$$E_B = E(\text{gas}) + E(\text{adsorbent}) - E(\text{adsorbent} + \text{gas}) \quad (5)$$

Data availability

All data supporting the findings of this study are available within this article and its Supplementary Information. Source data that support the findings of this study are available from the corresponding author upon reasonable request. Correspondence and requests for materials should be addressed to H.X.

References

1. Sholl, D. S. & Lively, R. P. Seven chemical separations to change the world. *Nature* **532**, 435–437 (2016).
2. Lin, J. Y. Molecular sieves for gas separation. *Science* **353**, 121–122 (2016).
3. Wu, Y. & Weckhuysen, B. M. Separation and purification of hydrocarbons with porous materials. *Angew. Chem. Int. Ed.* **60**, 18930–18949 (2021).
4. Adil, K. et al. Gas/vapour separation using ultra-microporous metal–organic frameworks: insights into the structure/separation relationship. *Chem. Soc. Rev.* **46**, 3402–3430 (2017).
5. Yang, L. et al. Energy-efficient separation alternatives: metal–organic frameworks and membranes for hydrocarbon separation. *Chem. Soc. Rev.* **49**, 5359–5406 (2020).
6. Liao, P.-Q. et al. Controlling guest conformation for efficient purification of butadiene. *Science* **356**, 1193–1196 (2017).
7. Wang, J. et al. Fine pore engineering in a series of isoreticular metal-organic frameworks for efficient C_2H_2/CO_2 separation. *Nat. Commun.* **13**, 1–8 (2022).
8. Hao, H. G. et al. Simultaneous trapping of C_2H_2 and C_2H_6 from a ternary mixture of $C_2H_2/C_2H_4/C_2H_6$ in a robust metal–organic framework for the purification of C_2H_4. *Angew. Chem. Int. Ed.* **130**, 16299–16303 (2018).
9. Wang, H. et al. Topologically guided tuning of Zr-MOF pore structures for highly selective separation of C6 alkane isomers. *Nat. Commun.* **9**, 1–11 (2018).
10. Shen, J. et al. Simultaneous interlayer and intralayer space control in two-dimensional metal–organic frameworks for acetylene/ethylene separation. *Nat. Commun.* **11**, 1–10 (2020).
11. Jiang, H. et al. A reticular chemistry guide for the design of periodic solids. *Nat. Rev. Mater.* **6**, 466–487 (2021).
12. Behera, N. et al. The chemistry and applications of flexible porous coordination polymers. *EnergyChem* **3**, 100067 (2021).
13. Yaghi, O.M. et al. *Introduction to Reticular Chemistry: Metal-organic Frameworks and Covalent Organic Frameworks* (John Wiley & Sons, 2019).
14. Zhang, Z. et al. Optimal pore chemistry in an ultramicroporous metal–organic framework for benchmark inverse CO_2/C_2H_2 separation. *Angew. Chem. Int. Ed.* **60**, 17198–17204 (2021).
15. Li, J. et al. Purification of propylene and ethylene by a robust metal–organic framework mediated by host–guest interactions. *Angew. Chem. Int. Ed.* **60**, 15541–15547 (2021).
16. Bereciartua, P. J. et al. Control of zeolite framework flexibility and pore topology for separation of ethane and ethylene. *Science* **358**, 1068–1071 (2017).
17. Lin, R.-B. et al. Molecular sieving of ethylene from ethane using a rigid metal–organic framework. *Nat. Mater.* **17**, 1128–1133 (2018).
18. Bao, Z. et al. Molecular sieving of ethane from ethylene through the molecular cross-section size differentiation in gallate-based metal–organic frameworks. *Angew. Chem. Int. Ed.* **130**, 16252–16257 (2018).
19. Ding, Q. et al. Exploiting equilibrium-kinetic synergetic effect for separation of ethylene and ethane in a microporous metal-organic framework. *Sci. Adv.* **6**, eaaz4322 (2020).
20. Zeng, H. et al. Orthogonal-array dynamic molecular sieving of propylene/propane mixtures. *Nature* **595**, 542–548 (2021).
21. Yu, L. et al. Pore distortion in a metal–organic framework for regulated separation of propane and propylene. *J. Am. Chem. Soc.* **143**, 19300–19305 (2021).
22. Wang, Y. et al. Selective aerobic oxidation of a metal–organic framework boosts thermodynamic and kinetic propylene/propane selectivity. *Angew. Chem. Int. Ed.* **131**, 7774–7778 (2019).
23. Yu, M.-H. et al. Enhanced gas uptake in a microporous metal–organic framework via a sorbate induced-fit mechanism. *J. Am. Chem. Soc.* **141**, 17703–17712 (2019).
24. Lyndon, R. et al. Tuning the structures of metal–organic frameworks via a mixed-linker strategy for ethylene/ethane kinetic separation. *Chem. Mater.* **32**, 3715–3722 (2020).
25. Cadiau, A. et al. A metal-organic framework–based splitter for separating propylene from propane. *Science* **353**, 137–140 (2016).
26. Wang, H. et al. Tailor-made microporous metal–organic frameworks for the full separation of propane from propylene through selective size exclusion. *Adv. Mater.* **30**, 1805088 (2018).
27. Cao, J.-W. et al. One-step ethylene production from a four-component gas mixture by a single physisorbent. *Nat. Commun.* **12**, 1–8 (2021).
28. Chen, K.-J. et al. Synergistic sorbent separation for one-step ethylene purification from a four-component mixture. *Science* **366**, 241–246 (2019).

29. Liang, B. et al. An ultramicroporous metal–organic framework for high sieving separation of propylene from propane. *J. Am. Chem. Soc.* **142**, 17795–17801 (2020).
30. Yang, H. et al. Pore-space-partition-enabled exceptional ethane uptake and ethane-selective ethane–ethylene separation. *J. Am. Chem. Soc.* **142**, 2222–2227 (2020).
31. Hartmann, M. et al. Adsorptive separation of olefin/paraffin mixtures with ZIF-4. *Langmuir* **31**, 12382–12389 (2015).
32. Pires, J. et al. Ethane selective IRMOF-8 and its significance in ethane–ethylene separation by adsorption. *ACS Appl. Mater. Interfaces* **6**, 12093–12099 (2014).
33. Gucuyener, C. et al. Ethane/ethene separation turned on its head: selective ethane adsorption on the metal–organic framework ZIF-7 through a gate-opening mechanism. *J. Am. Chem. Soc.* **132**, 17704–17706 (2010).
34. Pascual, P. et al. Development of a transferable guest-host force field for adsorption of hydrocarbons in zeolites. II. Prediction of alkenes adsorption and alkane/alkene selectivity in silicalite. *J. Phys. Chem. B* **108**, 393–398 (2004).
35. Li, L. et al. Ethane/ethylene separation in a metal-organic framework with iron-peroxo sites. *Science* **362**, 443–446 (2018).
36. Liao, P.-Q. et al. Efficient purification of ethene by an ethane-trapping metal-organic framework. *Nat. Commun.* **6**, 1–9 (2015).
37. Zeng, H. et al. Cage-interconnected metal–organic framework with tailored apertures for efficient C_2H_6/C_2H_4 separation under humid conditions. *J. Am. Chem. Soc.* **141**, 20390–20396 (2019).
38. Geng, S. et al. Scalable room-temperature synthesis of highly robust ethane-selective metal–organic frameworks for efficient ethylene purification. *J. Am. Chem. Soc.* **143**, 8654–8660 (2021).
39. Chen, C. X. et al. Nanospace engineering of metal–organic frameworks through dynamic spacer installation of multifunctionalities for efficient separation of ethane from ethane/ethylene mixtures. *Angew. Chem. Int. Ed.* **60**, 9680–9685 (2021).
40. He, C. et al. Modification of the pore environment in UiO-type metal-organic framework toward boosting the separation of propane/propylene. *Chem. Eng. J.* **403**, 126428 (2021).
41. Chen, Y. et al. An ethane-trapping MOF PCN-250 for highly selective adsorption of ethane over ethylene. *Chem. Eng. Sci.* **175**, 110–117 (2018).
42. Lin, R.-B. et al. Boosting ethane/ethylene separation within isoreticular ultramicroporous metal–organic frameworks. *J. Am. Chem. Soc.* **140**, 12940–12946 (2018).
43. Zhang, X. et al. Selective ethane/ethylene separation in a robust microporous hydrogen-bonded organic framework. *J. Am. Chem. Soc.* **142**, 633–640 (2019).
44. Zhang, X. et al. A rod-packing hydrogen-bonded organic framework with suitable pore confinement for benchmark ethane/ethylene separation. *Angew. Chem. Int. Ed.* **133**, 10392–10398 (2021).
45. Qazvini, O. T. et al. A robust ethane-trapping metal–organic framework with a high capacity for ethylene purification. *J. Am. Chem. Soc.* **141**, 5014–5020 (2019).
46. Su, K. et al. Efficient ethylene purification by a robust ethane-trapping porous organic cage. *Nat. Commun.* **12**, 1–7 (2021).
47. Xu, Z. et al. A robust Th-azole framework for highly efficient purification of C_2H_4 from a $C_2H_4/C_2H_2/C_2H_6$ mixture. *Nat. Commun.* **11**, 1–9 (2020).
48. Yang, L. et al. Polycatenated molecular cage-based propane trap for propylene purification with recorded selectivity. *ACS Appl. Mater. Interfaces* **12**, 2525–2530 (2019).
49. Hong, A. N. et al. Pore-space partition and optimization for propane-selective high-performance propane/propylene separation. *ACS Appl. Mater. Interfaces* **13**, 52160–52166 (2021).
50. Yang, S.-Q. et al. Propane-trapping ultramicroporous metal–organic framework in the low-pressure area toward the purification of propylene. *ACS Appl. Mater. Interfaces* **13**, 35990–35996 (2021).
51. Gu, Y. et al. Host–guest interaction modulation in porous coordination polymers for inverse selective CO_2/C_2H_2 separation. *Angew. Chem. Int. Ed.* **60**, 11688–11694 (2021).
52. Pei, J. et al. Engineering microporous ethane-trapping metal–organic frameworks for boosting ethane/ethylene separation. *J. Mater. Chem. A* **8**, 3613–3620 (2020).
53. Kang, M. et al. A robust hydrogen-bonded metal–organic framework with enhanced ethane uptake and selectivity. *Chem. Mater.* **33**, 6193–6199 (2021).
54. Peng, J. et al. Selectively trapping ethane from ethylene on metal–organic framework MIL-53 (Al)-FA. *Ind. Eng. Chem. Res.* **58**, 8290–8295 (2019).
55. Kang, M. et al. High-throughput discovery of Ni (IN) 2 for ethane/ethylene separation. *Adv. Sci.* **8**, 2004940 (2021).
56. Myers, A. L. & Prausnitz, J. M. Thermodynamics of mixed-gas adsorption. *AIChE J.* **11**, 121–127 (1965).
57. Krishna, R. Methodologies for screening and selection of crystalline microporous materials in mixture separations. *Sep. Purif. Technol.* **194**, 281–300 (2018).
58. Segall, M. et al. First-principles simulation: ideas, illustrations and the CASTEP code. *J. Phys. Condens. Mat.* **14**, 2717 (2002).

Acknowledgements

This work is supported by the Zhejiang Provincial Natural Science Foundation of China (No. LR20B060001), the National Natural Science Foundation of China (No. 22108240, 21725603, and 21938011), and the Research Computing Center in College of Chemical and Biological Engineering at Zhejiang University.

Author contributions

H.X., L.Y., X.C., and P.Z. conceived the project idea, designed the research, and co-wrote the manuscript. P.Z. carried out the materials synthesis, adsorption experiments, transient breakthrough measurements, and computational simulation. X.S. conducted the cycling breakthrough experiment. L.C. performed the IAST calculation. J.W. and X.L. contributed to the measurement of time-dependent gas uptake profiles. All authors contributed to the discussion of results and commented on the manuscript.

Competing interests

The authors declare no competing interests.

Additional information

Supplementary information The online version contains supplementary material available at https://doi.org/10.1038/s41467-022-32677-3.

Correspondence and requests for materials should be addressed to Huabin Xing.

Peer review information *Nature Communications* thanks Martin Hartmann, Banglin Chen and the other, anonymous, reviewer for their contribution to the peer review of this work.